Stellar He burning of ^{18}O: A measurement of low-energy resonances and their astrophysical implications

S. Dababneh,* M. Heil, and F. Käppeler
Forschungszentrum Karlsruhe, Institut für Kernphysik, 76021 Karlsruhe, Germany

J. Görres and M. Wiescher
University of Notre Dame, Department of Physics, Notre Dame, Indiana 46556, USA

R. Reifarth
Los Alamos National Laboratory, Los Alamos, New Mexico 87545, USA

H. Leiste
Forschungszentrum Karlsruhe, Institut für Materialforschung I, 76021 Karlsruhe, Germany

The ^{22}Ne(α,n) reaction is the main neutron source for neutron capture nucleosynthesis (*s* process) in massive stars and plays also a significant role for the *s* process in thermally pulsing asymptotic giant branch stars. In these scenarios, ^{22}Ne is produced by the reaction sequence ^{14}N(α,γ)^{18}F(β^+)^{18}O(α,γ)^{22}Ne. While the first reaction is well understood, α capture on ^{18}O was affected by considerable uncertainties. At the temperatures of stellar He burning, the reaction rate is determined by two resonances at α energies of 470 and 566 keV. Since these resonances were not yet successfully measured, the rates had to be based on estimated resonance strengths. In the present work, the first direct measurement of the partial strengths of these extremely weak low-energy resonances is reported. The use of a high-efficiency segmented Ge detector in coincidence with bismuth germanate oxide counters covering a large solid angle led to a significantly improved experimental sensitivity, thus allowing for the clear identification of specific γ transitions. As a result, resonance strengths of 0.71 ± 0.17 μeV and 0.48 ± 0.16 μeV could be obtained for the 566- and 470-keV resonances, respectively. When compared to the previously reported upper limits of ≤1.7 μeV, these results provide a reliable basis for the determination of the reaction rate during stellar He burning. Accordingly, these data reduce the uncertainties in the *s* process neutron balance.

I. INTRODUCTION

The "main" and the "weak" components of nucleosynthesis by the slow neutron capture process (*s* process) indicate that two separate sites contributed to the abundances of *s* nuclei [1]. The weak component is believed to be related to the production of nuclei up to Zr ($A<90$) during He burning in the cores of massive stars (≥15 M$_\odot$), while the main component ($A=90$–209) is likely to occur in the He-burning shell in low mass asymptotic giant branch (AGB) stars [2,3]. The ^{22}Ne(α,n) neutron source plays an important role in both scenarios. While this reaction dominates the neutron production in massive stars, the lower temperatures in low mass stars favor the ^{13}C(α,n) reaction that provides about 95% of the total neutron exposure. However, the final abundance patterns are modified in a characteristic way by the marginal activation of the ^{22}Ne(α,n) reaction at the end of each neutron production episode in thermally pulsing AGB stars [3]. At this evolutionary stage, recurrent He shell flashes lead to sufficiently high temperatures ($T_9\sim0.3$, in units of 10^9K) so that ^{22}Ne(α,n) reactions add typically 5%

to the total exposure, but at a much higher neutron density than in the previous ^{13}C(α,n) phase. Accordingly, the abundance patterns that we observe are strongly influenced by the ^{22}Ne(α,n) neutron source. It is this interplay between the complementary neutron sources, ^{13}C(α,n) and ^{22}Ne(α,n), which represents a persisting challenge for nuclear astrophysics, since both reactions are yet uncertain due to lack of data in the relevant temperature regions of the respective stellar sites. This work is devoted to an improved study of the reaction sequence leading to the buildup of ^{22}Ne during stellar He burning.

In the preceeding carbon-nitrogen-oxygen (CNO) driven hydrogen burning phase of massive stars, practically all of the CNO nuclei are transformed into ^{14}N, since proton capture on ^{14}N is the slowest reaction in the cycle. The ^{14}N ashes of hydrogen burning are converted to ^{22}Ne by the reaction sequence ^{14}N(α,γ)^{18}F(β^+)^{18}O(α,γ)^{22}Ne. The resulting ^{22}Ne abundance and hence the efficiency of the subsequent ^{22}Ne(α,n)^{25}Mg neutron source depend on the preceding α capture reactions on ^{14}N and ^{18}O. The reaction rates at the relevant temperatures are expected to be dominated by contributions of low-energy resonances [4]. While the first reaction is well understood [5], α capture on ^{18}O is still affected by considerable uncertainties.

Previous direct measurements of the ^{18}O(α,γ)^{22}Ne reaction covered the energy range from 0.6 to 2.3 MeV [6] and

---

*On leave from Faculty of Applied Sciences, Al-Balqa Applied University, Salt 19117, Jordan. Electronic address: saed.dababneh@ik.fzk.de

from 2.15 to 3.70 MeV [7]. Therefore, the stellar reaction rate is well determined by the available experimental data at temperatures $T_9 = 0.3$–4.3. At the relevant s process temperatures ($T_9 < 0.3$), however, the rate might be significantly enhanced if additional resonances could be detected at energies below 600 keV [6]. At these energies, penetration through the Coulomb barrier reduces the α width (Γ_α) sharply to values much less than the γ width ($\Gamma_\alpha \ll \Gamma_\gamma$) and the strength of these low-energy resonances thus depends only on Γ_α. It was indicated [6] that due to the $\omega\gamma = \omega\Gamma_\alpha$ dependence and due to the barrier penetration factor contained in Γ_α, the low-energy resonances were inaccessible to experiments aiming at a direct strength measurement. These possible resonance levels, which would dominate the reaction rate at astrophysical energies, have been so far studied only indirectly. The $^{18}O(^6Li,d)^{22}Ne$ α transfer reaction has been used to investigate the level structure of ^{22}Ne around the α threshold [8]. Attempts to measure these low-energy resonances directly could provide only upper limits for the resonance strengths [8,9]. The predicted resonance strengths are low (≤ 1.7 μeV) and are reported as extremely difficult to be accessed in direct measurements [4].

In general, there is a strong demand for reliable charged particle reaction rates for stellar nucleosynthesis calculations. The main problem is that these measurements are handicapped by high backgrounds, which include natural, cosmic ray induced, as well as beam induced components. Since background reduction and event suppression techniques are imperative for the investigation of extremely weak reactions [10], this work is aimed at improving the γ detection sensitivity, or in other words, at increasing the capture yield-to-background ratio.

With standard spectroscopy, background levels are overwhelmingly much higher than the expected yield from the weak resonances even with heavy passive shielding. By analysis of the different components in the background spectrum and of the expected transitions in the ^{22}Ne compound nucleus, the setup has been designed to selectively exclude all events that do not satisfy certain physical criteria characteristic of the sought transitions. The method utilizes high-efficiency bismuth germanate oxide (BGO) scintillators in coincidence with high resolution granular Ge detectors from which all information is recorded event by event for later off-line analysis. Since the decay of the resonant state, unlike common backgrounds, includes cascades of well defined γ lines, substantial background reduction could be achieved by means of the coincidence technique.

As a result, the detection sensitivity could be sufficiently enhanced to identify at least the first excited state to ground state transition in the compound nucleus ^{22}Ne for the resonances in the astrophysically relevant energy range, which to our knowledge are the weakest (α,γ) resonances ever directly measured.

II. EXPERIMENTAL METHOD

The experiment has been conducted at the Karlsruhe 3.7-MV Van de Graaff accelerator. The beam, guided through a Ta collimator and a LN_2-cooled Cu trap, was
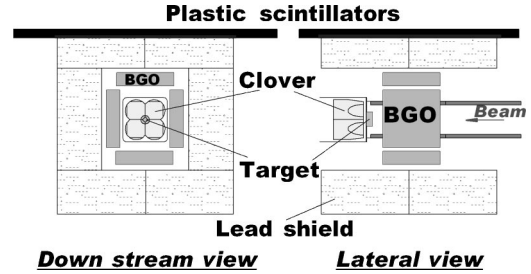

FIG. 1. Downstream and lateral views of the experimental setup are represented schematically.

swept horizontally and vertically across an effective target area of 1 cm^2 to illuminate the target homogeneously. The targets were mounted at 0° to the beam direction and were directly water cooled. Target and chamber formed a Faraday cup for measuring the integrated beam current on target. A negative voltage of 300 V was applied to the Cu trap to suppress secondary electron emission. Typical α-beam currents of $\sim$115 μA on target at energies above 600 keV were available, while at lower energies the current was limited to $\sim$70 μA.

The experimental setup was optimized in several steps and was eventually adopted in the version sketched in Fig. 1. The main component in the γ-detection system is the Eurisys Mesures Clover array placed at 0° to the beam direction. It consists of four coaxial n-type HPGe diodes 50 mm in diameter and 70 mm in length, cut in a way that enables close packing with a Ge-Ge distance of only 0.2 mm [11]. The crystals are mounted in a common cryostat. The total active Ge volume is 470 cm^3. The γ efficiency was determined from the known γ decay of the $^{27}Al(p,\gamma)^{28}Si$ resonance at 992 keV [12,13] and the known resonance strength of $\omega\gamma = (1.91 \pm 0.11)$ eV [14] as well as by calibrated sources. The second part of the γ-detection system consists of four Scionix BGO crystals, $13 \times 13 \times 3$ cm^3 in size, surrounding the upstream side of the target. The BGO detectors together with the plastic scintillator panels on top of the setup ($60 \times 50 \times 2$ cm^3) serve to provide coincident events that can be used for off-line background reduction. The passive lead shield consisted of a 10-cm-thick layer for reducing the ambient γ-ray background level. This geometry has been optimized for Clover-BGO coincidences. The final geometry adopted for the experimental setup has been modeled in detail by extensive GEANT4 [15] Monte Carlo simulations.

The signals from all detectors, i.e., from the energy outputs of the four Clover crystals, two energy outputs of the four BGO scintillators (each two coupled together), the Clover-BGO timing signals, as well as the Clover-plastic scintillator timing signals are processed and recorded event by event in an 8 analog-to-digital converter data acquisition system. No hardware vetos have been included, so that all necessary information is preserved for repeated and flexible software analysis.

If each crystal in the Clover detector is considered independently as a single detector, then the composite Clover detector is said to be operated in "direct" mode. Thus the photopeak detection efficiency is simply the sum of the individual photopeak efficiencies of each of the four crystals.

On the other hand, the close packing of the Clover detector facilitates its operation in the so called "addback" mode. In this mode, coincident events in different crystals are summed resulting in the reconstruction of full-energy signals if Compton-scattered and 511-keV annihilation photons escaping from one crystal are detected in another crystal. The summed signals are stored in the addback spectrum, which results in improved full-energy peak efficiency at the expense of the Compton continuum and escape peaks. In case of coincident cascade photons resulting from the decay of a highly excited nuclear state, summing effects may complicate the intensity calculation, since the observed yield depends not only on the detection efficiency for monoenergetic γ's but on the possibility of detecting coincident cascade photons as well. However, these effects are strongly reduced in the coincidence spectra. As implied by the geometry of the detection system, the coincidence spectrum includes selectively and by definition those transitions in the cascade that correspond to γ photons emitted in opposite directions. Detailed description of the different modes of operation of the detection system together with the Monte Carlo simulations are in preparation and will be published in a forthcoming paper [16]. The coincidence option is further described in conjunction with the study of the reference resonances in Sec. IV.

The ^{18}O targets have been prepared as $Al_2^{18}O_3$ films deposited onto 0.4-mm-thick Ta backings by reactive sputtering in an $Ar/^{18}O_2$ mixture at 0.4 Pa. The $^{18}O_2$ gas was of high purity, >99.9% in chemical composition and 96.6% in isotopic enrichment, and an aluminum disk of high purity (99.999%) has been used as the sputtering cathode. The same method has been used to prepare natural oxygen Al_2O_3 layers for background measurements.

The search for low-energy resonances has been performed using 95-μg/cm^{2}Al$_2^{18}$O$_3$ films. A target of the same thickness has been used to measure the resonance at $E_\alpha = 660$ keV. Thinner ^{18}O targets (~ 35 μg/cm^2) served to study the high-energy resonances at $E_\alpha = 750$ and 770 keV.

The stoichiometry of the targets was verified by measuring the strong ^{27}Al$(p,\gamma)^{28}$Si resonance at 992 keV with a pure Al target and an Al$_2$O$_3$ target. The observed ratio of the γ yields is in excellent agreement with the expectation for an Al$_2$O$_3$ stoichiometry.

The target stability was monitored during the experiments by investigating the yield from the 660-keV resonance of the ^{18}O$(\alpha,\gamma)^{22}$Ne reaction in steps of 1 C up to a total integrated charge of 14 C for an α beam of $\sim$120 μA on target (Fig. 2). The stability of the targets was also confirmed by measuring the ^{18}O$(p,\gamma)^{19}$F resonance yield at 1167 keV [17] before and after each of the long runs performed at low α energies.

III. THE RESONANCE AT $E_\alpha = 750$ keV

Although the resonance of the ^{18}O$(\alpha,\gamma)^{22}$Ne reaction at $E_\alpha = 750$ keV has been previously investigated [6,9,8], its decay properties have been examined in this work with improved accuracy. Since angular distribution measurements on this resonance indicate isotropic γ-emission [8], the spec-
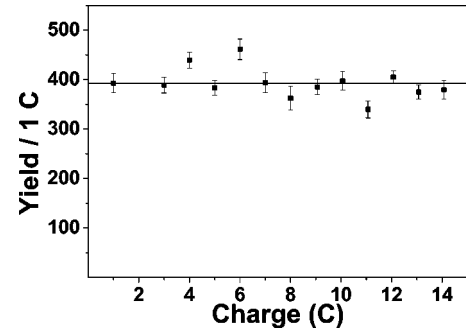

FIG. 2. Verification of the target stability using the 660-keV resonance of the ^{18}O$(\alpha,\gamma)^{22}$Ne reaction. The measured yield for the transition from the first excited state to the ground state is plotted against the accumulated charge.

trum taken with the current setup (Fig. 3) reveals new details about the decay modes and branching ratios. The direct mode spectrum acquired for an integrated beam current of 4.88 C has been analyzed, and the line intensities have been corrected for summing effects using the correction factor $[1 - (\bar{M}-1)\eta_T]^{-1}$, where $\bar{M}$ is the average multiplicity of the γ transition in the different cascades calculated from the branching ratios of the secondary transitions [12,13], and η_T is the average total efficiency for a single Ge crystal in the Clover array [16]. The intensity of each decay mode of the resonant state has been obtained from the analysis of the spectrum as the weighted average of the intensity of the corresponding primary transition and that of the observed secondaries. Table I lists the observed primary transitions and the corresponding branching ratios together with those found in the literature.

The previously available information on the resonance strength is 560 ± 60 μeV [9] and 470 ± 80 μeV [6]. Trautvetter *et al.* [6] determined the resonance strength of the 750-keV resonance relative to a resonance at 2.20 MeV, the strength of which was determined relative to the closely spaced doublet ($\Delta E_\alpha = 1.9$ keV) at $E_\alpha = 1.53$ MeV of the ^{14}N$(\alpha,\gamma)^{18}$F reaction. While the stopping power values used
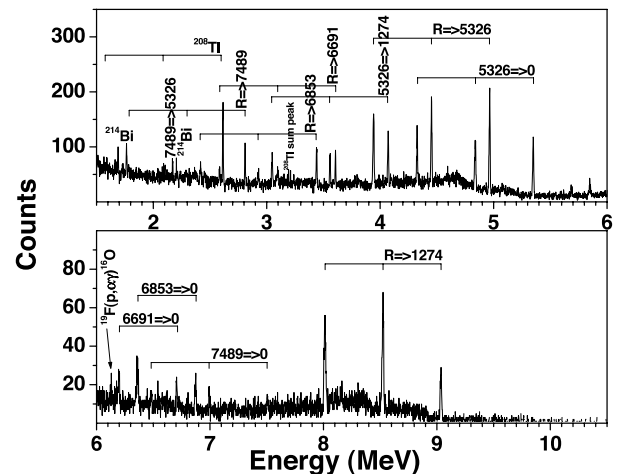

FIG. 3. Cosmic suppressed spectrum (direct mode) acquired for the 750 keV resonance for an integrated beam current of 4.88 C.

TABLE I. Branching ratios obtained in this work for the 750-keV resonance compared to those found in the literature.

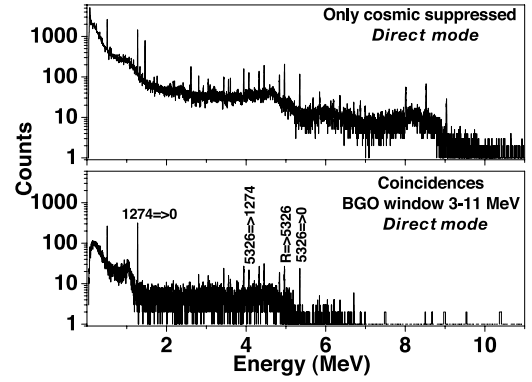| Primary transition	γ branch (%)		
	This work	Ref. [9]	Ref. [6]
$R \Rightarrow 7489\ (1^-)$	7.7±0.8	10±3	
$R \Rightarrow 6853\ (1^+)$	10.1±1.1	20±4	15±4
$R \Rightarrow 6691\ (1^-)$	7.1±1.1		
$R \Rightarrow 5326\ (1^+)$	46.6±2.5	44±5	55±4
$R \Rightarrow 1274\ (2^+)$	28.5±3.1	25±5	30±4

FIG. 4. The Ge Clover spectrum taken on the 750-keV resonance with an integrated beam current of 4.88 C. The top panel shows the situation if only the plastic scintillators covering the experimental setup are used for reduction of the secondary cosmic ray background. The bottom panel shows the coincidence spectrum obtained with a BGO window of 3–11 MeV where the cosmic component is also suppressed. The improvement in the peak-to-background ratio for the 1274-keV line is obvious.

in that determination were obtained from Ref. [18], more recent stopping power data [19] lead to a corrected resonance strength of $\omega\gamma = 390 \pm 70$ μeV. Similarly, the corresponding correction for the 660-keV resonance [6] leads to a revised value of $\omega\gamma = 240 \pm 40$ μeV (Table II).

From the total yield of $(1.56 \pm 0.12) \times 10^{-14}$ per incident particle obtained in this work, and using the effective stopping power $\varepsilon(\mathrm{Al}_2{}^{18}\mathrm{O}_3) = \varepsilon(^{18}\mathrm{O}) + \frac{2}{3}\varepsilon(\mathrm{Al}) = 79.5 \times 10^{-15}$ eV cm^2 [19], the total strength of the 750-keV resonance has been determined to be $\omega\gamma = 490 \pm 45$ μeV. The uncertainty in the resonance strength includes, in addition to the statistical uncertainty in the measured yield, the uncertainties in the detection efficiency, the total efficiency for the summing correction in direct mode, as well as the 5% uncertainty of the stopping power data. The weighted average of this measurement and the two previous values yields a resonance strength of $\omega\gamma = 490 \pm 40$ μeV (Table II).

IV. THE COINCIDENCE OPTION AND THE REFERENCE RESONANCES AT 660, 750, AND 770 keV

The determination of the strengths of the astrophysically important weak resonances at 566 and 470 keV is to be based on coincidences between the secondary transition (first

TABLE II. Parameters of the reference resonances in the $^{18}\mathrm{O}(\alpha,\gamma)^{22}\mathrm{Ne}$ reaction.

E_R (keV)[a]	E_x (keV)[b]	$J^{\pi c}$	$\omega\gamma(\mu eV)$	$\omega\gamma(\mu eV)^f$
662.1±1.0	10208.9	1^-	212±42[c]	229±19
			240±40[d]	
			230±25[a]	
749.9±1.0	10280.8	$0^+(1^-,2^+)$	560±60[a]	490±40
			390±70[d]	
			490±45[e]	
767.6±1.0	10295.3	2^+	1200±120[a]	1200±120

[a]Reference [9].
[b]Reference [13].
[c]Reference [8].
[d]Reference [6], corrected for stopping power values (Sec. III).
[e]This work (Sec. III).
[f]Used to calculate the contribution of the corresponding resonance to the total stellar reaction rate (Sec. VI) as well as a reference value to determine the strengths of the weak low-energy resonances (Sec. V).

excited state→ground state) detected in the Clover and primary transitions detected in the BGO's. These results will be normalized to the higher-energy reference resonances at 660, 750, and 770 keV. Accordingly, the coincidence techniques are discussed and applied to the reference resonances in this section. This sets the ground for the study of the low-energy resonances that will follow in Sec. V. The coincidence option using an energy window in the BGO data above 3 MeV was found to provide the best signal-to-background ratio. This window includes the primary transitions feeding the first excited state at 1274 keV. In spite of the reduction in the number of real counts in case of coincidences, the improved peak-to-background ratio allowed the identification of a clear peak for the 1274 keV line during the search for the low-energy resonances.

The improvement in the detection sensitivity of the 1274-keV line is illustrated in Fig. 4 for the 750-keV resonance. Though the peak efficiency in the coincidence spectrum (bottom panel) is reduced, the strong background suppression provides a convincing argument in favor of the coincidence option for detecting the much weaker yields anticipated for the low-energy resonances. Apart from the 1274-keV transition, several γ lines at higher energy, especially from a strong decay mode through the 5326-keV state (Table I) can be identified as well. The gain in peak-to-background ratio is shown in more detail in Fig. 5 for the energy region around the 1274-keV line. While the yield is lower by a factor 4.4 in the direct mode and 3.7 in the addback mode (left panel), the background is reduced by factors of 125 and 260 for the coincidence option, in the direct and addback modes, respectively (right panel). These ratios suggest that the addback, while not required for the high-energy resonances where the statistics in the direct mode are sufficient, will be helpful in case of the much weaker low-energy resonances. As discussed earlier, the addback mode suffers from uncertainties due to summing effects. However, these effects are strongly reduced in the coincidence spectra. As implied by the geom-
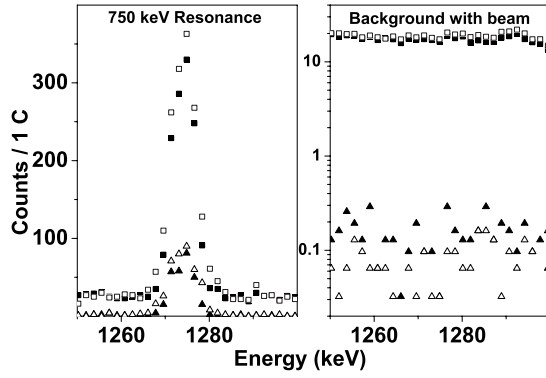
FIG. 5. Left panel: Same as in Fig. 4, but zoomed on the 1274-keV transition from the first excited to the ground state. Right panel: The same energy region is shown for the background run using a natural Al$_2$O$_3$ target. Both spectra correspond to a collected charge of 1 C. The squares correspond to the spectra in which only the secondary cosmic ray background component is suppressed while the triangles represent the Clover coincidence spectra with a 3–11 MeV window in the BGO data. Closed and open symbols correspond to the direct and addback modes, respectively.

etry of the detection system, the coincidence spectrum includes selectively and by definition those transitions in the cascade that correspond to γ photons emitted in opposite directions. That holds, in particular, for two step cascades which contribute 100%, 55%, and 75% to the total decays feeding the 1274-keV level, for the resonances at 660, 750, and 770-keV, respectively.

The different decay modes of any resonance in this reaction can be classified as in the upper right panel of Fig. 6. The coincidence option discussed so far considers modes 1 and 2, and a bypass correction is needed to account for the contribution of the other two modes in the calculation of the resonance strength. It would be necessary to consider mode 3 in the coincidence option in order to correct for the above
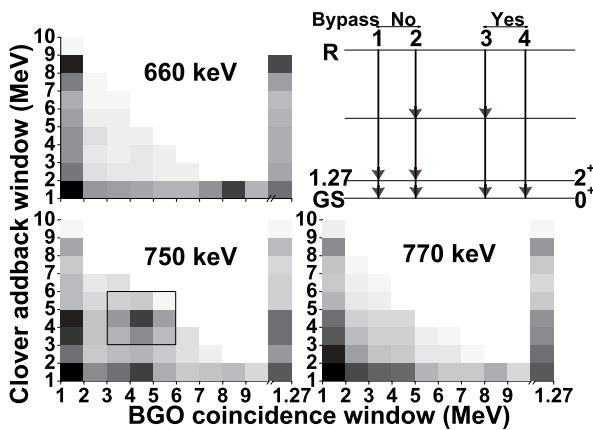

FIG. 6. Matrix spectra constructed for the three high-energy resonances. A clear "peak" in the 3–6 MeV region (both Clover and BGO) for the 750-keV resonance is consistent with the strong mode 3 transitions for this resonance. The rightmost column in each matrix represents coincidences in a BGO window around the 1274-keV line. The different modes of decay for a resonant state are summarized in the upper right panel.

mentioned bypasses over the first excited state. Obviously, mode 4 cannot be accounted for in this respect since the decay goes directly to the ground state. However, this mode is expected to contribute to the total yield only in the decay of resonances with spin ($J^\pi = 1^-$).

The rather important contribution of decay mode 3 cannot be obtained from the singles spectra in case of the weak yield anticipated for the low-energy resonances, where no identifiable γ lines can be measured. In order to investigate the relative contribution of this decay mode in an alternative way, three-dimensional coincidence "matrix" spectra have been constructed for each resonance. These matrices (Fig. 6) give the number of events in 1-MeV energy bins in the addback Clover spectrum which are in coincidence with 1-MeV energy bins in the BGO data. Since mode 3 decays bypassing the first excited state are characterized mainly by γ lines in the 3–6 MeV energy range, the corresponding 3×3 MeV region in the matrices gives, at least qualitatively, an idea about mode 3 bypasses. It should be noted that mode 2 also could contribute to this region. A "peak" inside this "square" is clearly seen in the 750-keV resonance matrix which is consistent with the mode 3 bypasses anticipated from its decay scheme. From the branching ratios obtained in this work for the primary transitions (Sec. III) and those for the secondaries [12,13], the contribution of mode 3 is (49 ±4)% of the total decay modes for this resonance.

The absolute efficiency η_{coin} for detecting the 1.27-MeV transition in coincidence with the 3–11 MeV BGO energy window can be calculated from the adopted strengths of the known resonances at 660, 750, and 770 keV (Table II) and the feeding probability B of the first excited state calculated from the known branching ratios (column 3 of Table III) using the relation

$$\omega\gamma = \frac{Y_{coin}}{\eta_{coin}} \frac{2\varepsilon}{\lambda^2} \frac{18}{22} \frac{1}{B}, \qquad (1)$$

where ε is the effective stopping power of α particles in the Al$_2$^{18}O$_3$ target $[=\varepsilon(^{18}\text{O}) + \frac{2}{3}\varepsilon(\text{Al})]$, λ is the center of mass wavelength, Y_{coin} is the coincidence yield per incident α particle. The results are listed in the last column of Table III along with the adopted weighted average of (0.80±0.07)%. Although the three reference resonances have different decay branchings and angular correlations, the uncertainty in the weighted average of the coincidence detection efficiency is constant within 9%. This can be explained by the large detection angles covered by the Clover and BGO detectors (Fig. 1) (for details, see Ref. [16]).

V. THE RESONANCES AT STELLAR ENERGIES

The techniques described above are applied to the low-energy resonances (<600 keV) in order to measure their resonance strengths, including additional fine tuning for the coincidence calculation.

A. Previous attempts

Trautvetter *et al.* [6] measured the ^{18}O(α,γ)^{22}Ne reaction in the energy range from 0.6 to 2.3 MeV. Their astrophysical

TABLE III. Net counts in the 1274-keV line in coincidence with a 3–11 MeV BGO window, and the corresponding absolute coincidence detection efficiency for the three high-energy resonances. The feeding probability (B) has been used to correct for bypasses over the first excited state.

Resonance energy (keV)	Coincidences (Counts / 1 C)	B (%)	Absolute coincidence efficiency (%)
750	364±9	51.5±4.2[a]	0.73±0.09
660	100±3	20.0±3.5[b]	0.97±0.20
770	1582±28	75.7±7.7[c]	0.90±0.14
		Average coincidence efficiency	0.80±0.07

[a]Calculated from the branching ratios of the primary transitions measured in this work and of the secondaries [12,13].

[b]Weighted averages of 17±5 [9] and 23±5 [6]. The only transition feeding the first excited state is the direct decay of the resonant state.

[c]Calculated from the branching ratios of the primary transitions [9] and of the secondaries [12,13].

reaction rate includes the contribution of the resonances in this energy range, as well as contributions of the direct capture process, the wings of a broad resonance at 1.53 MeV, and results from a previous work [7] that covered the energy range from 2.15 to 3.70 MeV. The compilation by Caughlan and Fowler CF88 [20] basically adopted their result [6] but included an estimate for the resonance at 58 keV. The stellar reaction rate is well determined by these experimental data at temperatures $T_9 = 0.3$–4.3. Below $T_9 = \sim 0.3$, however, the rate was expected to be significantly enhanced if additional resonances could be detected at energies below 600 keV [6,21].

In a later study, Giesen *et al.* [8] used the ^{18}O(^{6}Li,d)^{22}Ne α-transfer reaction to study the level structure of ^{22}Ne in the excitation range $E_x = 8.5$–11.3 MeV in search for α-unbound natural parity states. Four states were observed in that experiment at 9.72, 9.85, 10.05, and 10.13 MeV, corresponding to resonances at $E_\alpha = 58$, 218, 470, and 566 keV in the ^{18}O(α,γ)^{22}Ne reaction. From their angular distribution measurements of the transfer reaction, they obtained information on the possible angular momentum transfer l to the

populated states in ^{22}Ne. Possible spin assignments for these levels were also obtainable, since for these natural parity states the spin and parity are determined uniquely by $J = l$ and $\pi = (-1)^l$. The angular distribution measurement did not allow, however, for the assignment of unique l values. Therefore, the J^π assignment for these states remained ambiguous [22]. The available data are listed in Table IV. The resonance strengths in this table were calculated relative to the known 660-keV reference resonance using the relation

$$\omega\gamma = \frac{(2J+1)S_\alpha^l(E_x)P_l(E_\alpha)}{(2J_R+1)S_\alpha^l(E_x^R)P_l(E_\alpha^R)}\omega\gamma_R, \qquad (2)$$

where S_α^l is the α-spectroscopic factor and P_l is the penetrability through the Coulomb and orbital momentum barriers. The uncertain spin assignments for one single resonance create large variations in the corresponding calculated resonance strengths, emphasizing the need to measure the resonances directly. An attempt was made by Vogelaar *et al.* [9] using four large-volume NaI detectors in 4π geometry and

TABLE IV. Low-energy resonance parameters found in the literature.

E_α (keV)	E_x (MeV)	J^{π} [a]	S_α(%)	$\omega\gamma$ (μeV) Using Eq. (2) [22]	Experimental upper limit [8]	Experimental upper limit [9]
58	9.72	3^-	1.1	4.1×10^{-40}		
		(2^+)	2.5	1.5×10^{-39}		
218	9.85	2^+	1	7.1×10^{-12}		
		(1^-)	2.7	5.8×10^{-11}		
470	10.05	0^+	15	0.55	≤1.7	≤(0.0±0.2)
		(1^-)	4.7	0.23		
566	10.13	4^+	0.85	7.9×10^{-3}	≤1.7	≤(2.0±0.5)
		(2^+)	1.9	1.95		
		(3^-)	1	0.15		
662[b]	10.21	1^-	3.5	230±25		

[a]The first assignment for each resonance was adopted by Giesen *et al.* [8].

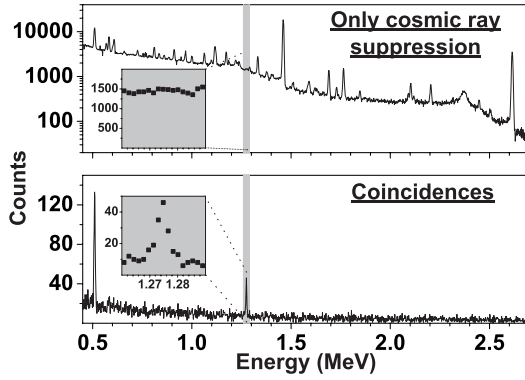[b]Reference resonance used in Eq. (2).

FIG. 7. Top: The spectrum for the combined runs at $E_\alpha = 600$, 620, and 640 keV with 87.5 C total integrated current and 213 h of beam time on target. These runs were carried out in search of the weak resonance at 566 keV. The secondary cosmic ray background component is suppressed in this spectrum and the appearing γ lines correspond to the background contributions. The shaded area represents the energy region where the first excited state transition is expected. Bottom: The corresponding coincidence spectrum illustrates the strong improvement of the peak-to-background ratio allowing the clear detection of the 1274-keV transition in the very weak 566-keV resonance.

by Giesen *et al.* [8] using a large Ge detector (35%) in close geometry with the target. While the results of the earlier measurement by Trautvetter *et al.* [6] for the resonances above 600 keV were confirmed, the measurements failed in detecting any of the lower resonances, and only upper limits for the strengths of the low-energy resonances could be obtained (Table IV).

B. The 566-keV resonance

Al$_2$O$_3$ targets 95 μg/cm^2 in thickness (corresponding to 120 keV energy loss of the α beam at 600 keV) have been used in search of the resonance reported by Ref. [8] at 566 keV. Typical α beam currents of $\sim$115 μA on target at energies of 600, 620, and 640 keV were available. Background measurements have been carried out at $E_\alpha = 620$ keV using natural oxygen Al$_2$O$_3$ targets of the same thickness.

The coincidence spectrum (BGO window 3–11 MeV) for the combined runs at 600, 620, and 640 keV and for an integrated beam current of 87.5 C is shown in the lower panel of Fig. 7. It illustrates the clear and unambiguous detection of the 1274 keV transition from the first excited state to the ground state, which has never been detected before. The upper panel of the figure shows the spectrum for the same runs but for which only the cosmic ray background component is suppressed. The γ-lines appearing in this spectrum correspond to the different room background contributions. The region of the spectrum around the 1274-keV line is further illustrated in Fig. 8 for this low-energy resonance as well as for the corresponding background spectrum (31 C) acquired at $E_\alpha = 620$ keV using the natural oxygen target. Figures 7 and 8 demonstrate how the real events immersed in the overwhelming room background are "picked out" by making use of the coincidence option. The net counts under the 1274-keV line in this addback coincidence spectrum of
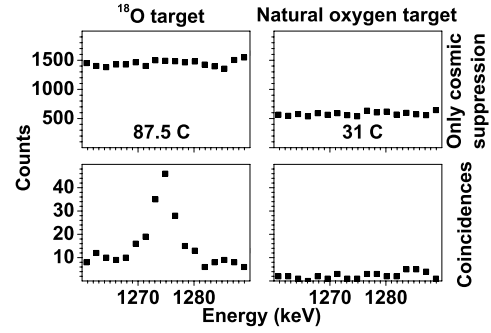

FIG. 8. Top: The region of the spectrum, with only cosmic ray background suppression, around the 1274-keV line for the low-energy resonance (566 keV) as well as for the background measured with a natural oxygen target. Bottom: The corresponding spectra with the coincidence option. The first excited state to ground state transition for the 566-keV resonance can be clearly identified in the coincidence spectrum. All spectra are in the addback mode.

117 ± 14 yields an average of 1.34 ± 0.16 counts per 1 C.

Using this result, along with the average absolute coincidence detection efficiency $\eta_{coin} = 0.80 \pm 0.07$ described in Sec. IV (Table III), the partial strength of the 566-keV resonance has been calculated according to

$$\omega\gamma_{partial} = \frac{Y_{coin}}{\eta_{coin}} \frac{2\varepsilon}{\lambda^2} \frac{18}{22}, \tag{3}$$

where ε is the stopping power and Y_{coin} is the coincidence yield per incident particle. The result is $\omega\gamma = 0.63 \pm 0.09$ μeV (Table V). The uncertainty includes a 5% error in the stopping power in addition to the uncertainties in the coincidence yield and efficiency. This partial strength is a lower limit for the total strength of this resonance and does not account for the transitions which bypass the first excited state at 1.27 MeV. However, this resonance has a spin $J^\pi = 2^+$ [25] and strong ground state transitions have been observed only for 1^- states in ^{22}Ne [12,13]. Information about the fraction of mode 3 decays (see Sec. IV) can be obtained from the present data.

From the branching ratios obtained in this work (Sec. III) for the 750-keV resonance, those listed by Vogelaar *et al.* [9] for the 770-keV resonance, and the available information [9,6] for the 660 keV resonance, the relative contributions of

TABLE V. Resonance strengths used to calculate the stellar reaction rate compared to NACRE [24]. All other resonances not listed are the same as in NACRE. The experimental partial strengths obtained in this work for the two low-energy resonances are also given.

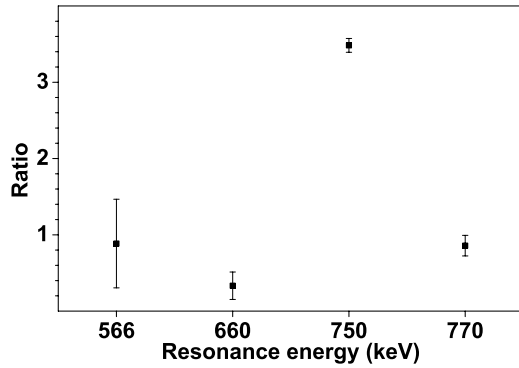| Resonance energy (keV)	$\omega\gamma_{partial}$ (μeV) This work	$\omega\gamma$ (μeV) This work	NACRE [24]
470	0.24 ± 0.08	0.48 ± 0.16	0.6
566	0.63 ± 0.09	0.71 ± 0.17	0.01
660		229 ± 19	239 ± 23
750		490 ± 40	530 ± 50

FIG. 9. The ratio between the net number of coincidences (3–6 MeV windows in both, Clover and BGO) to the net number of first excited state Clover coincidences (BGO window 3–11 MeV). This comparison examines the contribution of mode 3 decays that bypass the first excited state.

mode 3 decays have been calculated and found to be $(49 \pm 4)\%$, $(24 \pm 8)\%$, and $<4\%$ for the three resonances, respectively. Accordingly, the net number of coincident events in the 3 MeV$\times$3 MeV area (defined in Sec. IV) has been calculated and compared to the net 1274-keV γ's that are in coincidence with a 3–11 MeV BGO window (modes 1 and 2). The results are shown in Fig. 9. It should be emphasized here that mode 2 could also contribute to the 3 MeV$\times$3 MeV zone in the matrix spectrum. This suggests that mode 3 decays contribute less than 20% to the total resonance strength. This is supported by the fact that for all known 2^+ resonances, no strong mode 3 decays were observed [12,13]. For this reason, we estimate a partial strength for the mode 3 decay of 0.08 ± 0.08 μeV, leading to a total resonance strength of 0.71 ± 0.17 μeV which we adopt to calculate the corresponding stellar reaction rate (Sec. VI).

C. The 470 keV resonance

The attempt to directly measure the low-energy resonance at 470 keV has been affected by the lower beam currents, which was limited to $\sim$70 μA at α-particle energies of 530 keV. The coincidence spectrum obtained at this energy is
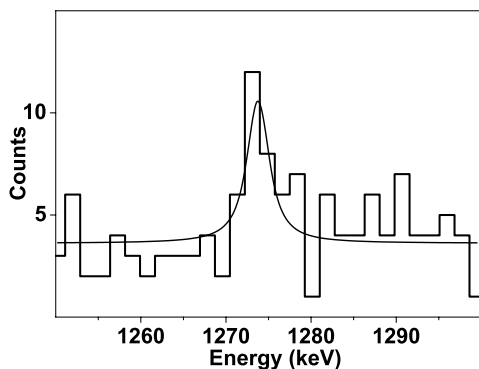

FIG. 10. The coincidence spectrum (BGO window 3–11 MeV) obtained in search of the 470-keV resonance for 33.3 C of integrated beam current. The counting statistics are limited because of the low beam current. The curve is a fit of the 1274-keV transition.

shown in Fig. 10. The clear feature in this spectrum, which corresponds to the 1274-keV transition, was never seen before. The background corrected net area of this line is 20.6 $\pm$7.9 for 33.3 C of integrated current. The same region of the spectrum shown in Fig. 10 has been further analyzed using the maximum likelihood estimate (MLE) and Poisson statistics [23]. Investigating the spectra of the high-energy resonances in the addback mode, the average full width at half maximum of the 1274-keV line is 3.8 channels corresponding to σ=1.6 channels. Using the MLE for Poisson statistics and the code POISSONMLE [23], the total signal for the 470-keV resonance is estimated as 20.7$\pm$6.3 counts with 68.5% confidence level. This result is in excellent agreement with the background subtracted net area mentioned above and yields a value of 0.62 ± 0.19 counts per 1 C of integrated beam current. It should be noted here that when the MLE is applied to the background spectrum measured with a natural oxygen target, it yields an upper limit of 0.18 counts per 1 C. Using the absolute coincidence detection efficiency and Eq. (3), the partial strength is 0.24 ± 0.08 μeV for the resonance at 470 keV, where the uncertainty includes, in addition to the uncertainties in the coincidence yield and efficiency, a 5% error in the stopping power.

Further detailed coincidence analyses such as those applied for the 566-keV resonance have been found to be not possible due to the large uncertainties. The spin of this resonance is not uniquely known, 0^+ or 1^- [8]. For this reason, a large branching to the ground state cannot be excluded. A typical branching ratio of 50% has been adopted from a comparison with the known branchings of 1^- states in ^{22}Ne [12,13]. This leads to a total resonance strength of 0.48 $\pm$0.16 μeV.

The estimates found in the literature for the strength of this resonance suffer from large uncertainties (Table IV). This applies, in particular, to the upper limits reported by Ref. [8] and Ref. [9] of $\leq$1.7 and $\leq(0.0\pm0.2)$ μeV, respectively. In such cases, the compilations of reaction rates [20,24] usually assume 10% of the upper limit for an estimate of the resonance strength. The values obtained from the angular distribution of the ^{18}O(^{6}Li,d)^{22}Ne transfer reaction [8,22] could, however, be compared to this measurement if the resonant level is populated with other reactions in a future experiment aiming at measuring the branching ratios and consequently determining the feeding probability of the first excited state. In addition, and given the excellent performance of the present setup and the remarkable stability of the sputtered targets, there is a good chance to arrive at an improved quantitative result for the 470-keV resonance, if the measurement is repeated at a dedicated facility, where high α-beam currents can be realized at low energies as well.

VI. ASTROPHYSICAL IMPLICATIONS

Because of the fairly high level density, the stellar rate of the ^{18}O(α,γ) reaction is entirely determined by single resonances, while the nonresonant reaction component can be neglected [20,8,22,24]. For a given temperature, the stellar reaction rate per particle pair for a narrow resonance is [21]

$$\langle \sigma v \rangle = \left(\frac{2\pi}{\mu kT} \right)^{3/2} \hbar^2 (\omega\gamma)_R \exp\left(\frac{-E_R^{\text{c.m.}}}{kT} \right). \qquad (4)$$

For several narrow resonances, the total reaction rate is simply the sum over the contributions of the single resonances. In units of reactions per s^{-1} mol^{-1} cm^3, the reaction rate as a function of temperature T_9 is [22]

$$N_A\langle \sigma v \rangle = 1.54$$

$$\times 10^5 (\mu T_9)^{-3/2} \sum_i (\omega\gamma)_i \exp\left(\frac{-11.604 E_{Ri}^{\text{c.m.}}}{T_9} \right), \qquad (5)$$

where $E_{Ri}^{\text{c.m.}}$ are the center of mass energies of the resonances in MeV, $(\omega\gamma)_i$ are the corresponding resonance strengths (in eV), and μ is the reduced mass (in amu).

It should be noted that from the angular distribution of the transfer reaction [8], the spin assignment for the level corresponding to the 566-keV resonance could indeed be $J^\pi = 2^+$ instead of 4^+ as adopted by Käppeler *et al.* [22] and by NACRE [24]. Also Mao and Fortune [25] reported this level with a $J^\pi = 2^+$ assignment. In this case, the resonance strength would be 1.95 μeV instead of 7.9×10^{-3} μeV [22] (or 0.01 μeV [24]), resulting in a more significant contribution to the reaction rate. This argument is confirmed by the results of the present measurement (Sec. V B). Recalling the partial strength (Table V) for the 566-keV resonance along with the recommended value of 0.71 ± 0.17 μeV (Sec. V B), we can thus exclude the $J^\pi = 4^+$ assignment and confirm the 2^+ character of this resonance. The upper limit of (2.0 ± 0.5) μeV suggested by Vogelaar *et al.* [9] (Table IV) also supports this conclusion.

The results obtained for the 470-keV resonance, on the other hand, cannot be interpreted so easily. As discussed before, the uncertainties due to the weak beam currents attainable at 530 keV do not allow for a reasonably precise conclusion about the resonance strength. This resonance strongly influences the reaction rate at the temperatures of interest. Unfortunately, though the coincidence method has proved to be effective in solving the ambiguity in the 566-keV resonance, the measurement of the weaker resonance at 470 keV still needs to be improved. Nevertheless, we have obtained a value of 0.48 ± 0.16 μeV for the strength of this resonance (see Fig. 10 and the related discussion in Sec. V C).

The strengths of the two low-energy resonances as well as for the reference resonances that are used in this work to
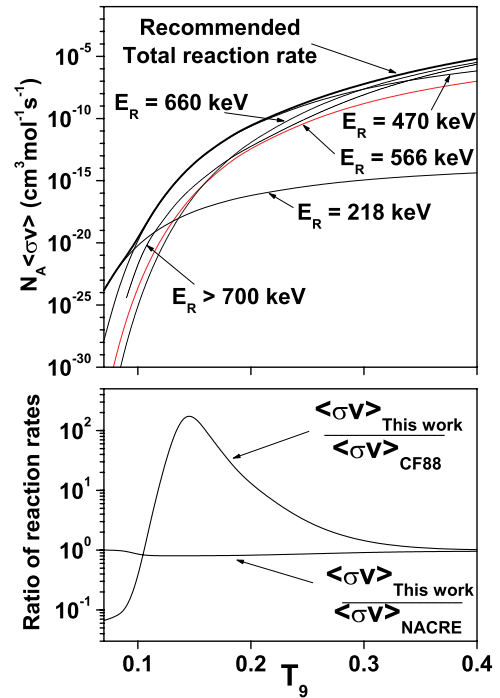

FIG. 11. Stellar reaction rates based on this work (top) compared to previous attempts (bottom).

calculate the stellar reaction rate are listed in Table V. The contribution of all other resonances not listed in the table are the same as in the NACRE compilation [24]. The stellar reaction rate based on the results of this work is shown in Fig. 11. Comparison with the literature is shown in the lower panel. The present rate confirms the strong enhancement (relative to CF88 [20]) at He-burning temperatures suggested by Käppeler *et al.* [22] and by the NACRE compilation [24].

At high temperatures ($T_9 \gtrsim 0.3$), the reaction rate is determined by the 660-keV and higher-energy resonances (Fig. 11). In the temperature range of stellar He-burning scenarios ($T_9 = 0.1 - 0.3$), the rate is dominated by the low-energy resonance at 470 keV. Clearly, the rate is much more sensitive to the 470-keV resonance than to the 566-keV resonance.

The total reaction rate and the contributions of the 470- and 566-keV resonances are also given in tabular form (Table VI). The temperature steps are the same as in CF88 and NACRE.

The total reaction rate for $T_9 \le 6$ is given by the analytical approximation:

$$N_A\langle \sigma v \rangle = 1.95 \times 10^{-13} T_9^{-3/2} \exp(-2.069/T_9) + 1.248 \times 10^{-2} T_9^{-3/2} \exp(-4.462/T_9)$$

$$+ 1.845 \times 10^{-2} T_9^{-3/2} \exp(-5.373/T_9) + 5.95 T_9^{-3/2} \exp(-6.285/T_9) + 12.74 T_9^{-3/2} \exp(-7.119/T_9)$$

$$+ 31.19 T_9^{-3/2} \exp(-7.287/T_9) + 3.22 \times 10^5 T_9^{-0.5} \exp(-21.801/T_9), \qquad (6)$$

where the rate is again given in cm^3 mol^{-1} s^{-1}.

TABLE VI. The total reaction rate (cm^3 mol^{-1} s^{-1}) and the contribution of the 470- and 566-keV resonances as a function of temperature $T_9(=10^9$ K).

T_9	470 keV	566 keV	Total
0.07	$1.40E-28$	$4.63E-34$	$1.53E-24$
0.08	$3.31E-25$	$5.56E-30$	$5.07E-23$
0.09	$1.36E-22$	$8.11E-27$	$8.86E-22$
0.10	$1.66E-20$	$2.71E-24$	$2.32E-20$
0.11	$8.29E-19$	$3.10E-22$	$8.83E-19$
0.12	$2.14E-17$	$1.60E-20$	$2.19E-17$
0.13	$3.31E-16$	$4.43E-19$	$3.38E-16$
0.14	$3.44E-15$	$7.59E-18$	$3.51E-15$
0.15	$2.59E-14$	$8.84E-17$	$2.65E-14$
0.16	$1.51E-13$	$7.53E-16$	$1.55E-13$
0.18	$2.81E-12$	$2.63E-14$	$2.94E-12$
0.20	$2.86E-11$	$4.45E-13$	$3.11E-11$
0.25	$1.77E-09$	$6.85E-11$	$2.55E-09$
0.30	$2.64E-08$	$1.87E-09$	$6.70E-08$
0.35	$1.75E-07$	$1.92E-08$	$8.86E-07$
0.40	$7.06E-07$	$1.07E-07$	$6.86E-06$
0.45	$2.04E-06$	$3.99E-07$	$3.50E-05$
0.50	$4.70E-06$	$1.12E-06$	$1.30E-04$
0.60	$1.58E-05$	$5.13E-06$	$9.44E-04$
0.70	$3.63E-05$	$1.46E-05$	0.004
0.80	$6.60E-05$	$3.12E-05$	0.011
0.90	$1.03E-04$	$5.52E-05$	0.024
1.00	$1.44E-04$	$8.57E-05$	0.045

VII. CONCLUSION

The ^{18}O$(\alpha,\gamma)^{22}$Ne reaction at low energies is of considerable astrophysical interest, since it determines the role of the important neutron source ^{22}Ne(α,n) for *s*-process nucleosynthesis. However, the astrophysically relevant resonances in this reaction at 566 and 470 keV are difficult to measure due to their extremely low resonance strengths.

The present work describes a successful experimental approach that results in the detection, for the first time, of yield from such weak resonances and consequently the determination of their strengths. Corrections for the different decay schemes of the resonant states have been carefully investigated and are discussed in detail. These are the weakest resonances ever directly measured. This experimental success has been achieved by a carefully designed spectrometer, which has been optimized for strong background suppres-

sion. The combination of the high resolution Ge Clover detector and the high-efficiency BGO scintillators was instrumental for achieving the required detection sensitivity for investigating the very weak resonances at astrophysical energies. The remarkable stability of the sputtered targets under the thermal load of high beam currents is an additional parameter contributing to the success of the measurement.

The exponential term in Eq. (4) implies that resonances with energies near kT will determine the reaction rate for a given stellar temperature [21]. For temperatures of stellar He burning, the energies and strengths of the low-energy resonances are, therefore, extremely important. In particular, the 470-keV resonance dominates in this temperature region (see Table VI). Based on the results of the present work, the determination of the strength of the 566-keV resonance reduces considerably the previous uncertainties in its contribution to the total reaction rate. The sensitivity of the present experiment is sufficient to deduce the contribution of the weaker resonance at 470 keV as well. If repeated with α-particle beams of an intensity comparable to that used to measure the 566-keV resonance, it is expected that this result can be further improved. A supplementary experiment to populate the two resonant states using other reactions in order to measure the branching ratios of their decays, and thus to deduce the feeding probabilities of the first excited state, would be helpful to confirm the present assumptions.

With these experimental results, the reaction rate could be quantified reliably and has been found to be higher compared to previous estimates by Caughlan and Fowler [20]. We confirm the strong enhancement at He-burning temperatures suggested by Giesen *et al.* [8], Käppeler *et al.* [22], and by the NACRE compilation [24].

[1] F. Käppeler, Prog. Part. Nucl. Phys. **43**, 419 (1999).
[2] B. Meyer, Annu. Rev. Astron. Astrophys. **32**, 153 (1994).
[3] R. Gallino, C. Arlandini, M. Busso, M. Lugaro, C. Travaglio, O. Straniero, A. Chieffi, and M. Limongi, Astrophys. J. **497**, 388 (1998).
[4] F. Käppeler, F.-K. Thielemann, and M. Wiescher, Annu. Rev. Nucl. Part. Sci. **48**, 175 (1998).
[5] J. Görres, C. Arlandini, U. Giesen, M. Heil, F. Käppeler, H.

Leiste, E. Stech, and M. Wiescher, Phys. Rev. C **62**, 055801 (2000).
[6] H. Trautvetter, M. Wiescher, K. Kettner, C. Rolfs, and J. Hammer, Nucl. Phys. **A297**, 489 (1978).
[7] A. Adams, M. Shapiro, W. Denny, E. Adelberger, and C. Barnes, Nucl. Phys. **A131**, 430 (1969).
[8] U. Giesen, C. Browne, J. Görres, J. Ross, M. Wiescher, R.E. Azuma, J. King, and M. Buckby, Nucl. Phys. **A567**, 146

(1994); U. Giesen, Ph.D. thesis, University of Notre Dame, 1992.

[9] R. Vogelaar, T. Wang, S. Kellogg, and R. Kavanagh, Phys. Rev. C **42**, 753 (1990).

[10] M. Wiescher, Nucl. Phys. **A688**, 241c (2001).

[11] G. Duchêne, F. Beck, P. Twin, G. de France, D. Curien, L. Han, C. Beausang, M. Bentley, P. Nolan, and J. Simpson, Nucl. Instrum. Methods Phys. Res. A **432**, 90 (1999).

[12] P. Endt, Nucl. Phys. **A521**, 1 (1990).

[13] P. Endt, Nucl. Phys. **A633**, 1 (1998).

[14] B. Paine and D. Sargood, Nucl. Phys. **A331**, 389 (1979).

[15] GEANT4 Collaboration, the GEANT4 Monte Carlo toolkit for the simulation of the passage of particles through matter, http://wwwinfo.cern.ch/asd/geant4/geant4.html

[16] S. Dababneh *et al.*, Nucl. Instrum. Methods Phys. Res. A (to be submitted).

[17] D. Tilley, H. Weller, C. Cheves, and R. Chasteler, Nucl. Phys. **A595**, 1 (1995).

[18] L. Northcliffe and R. Schilling, Nucl. Data Tables **A7**, 233 (1970).

[19] J. Ziegler and J. Biersack, SRIM 2000, The Stopping and Range of Ions in Matter, http://www.srim.org

[20] G. Caughlan and W. Fowler, At. Data Nucl. Data Tables **40**, 283 (1988).

[21] C. Rolfs and W. Rodney, *Cauldrons in the Cosmos* (University of Chicago Press, Chicago, 1988).

[22] F. Käppeler, M. Wiescher, U. Giesen, J. Görres, I. Baraffe, M. El Eid, C. Raiteri, M. Busso, R. Gallino, M. Limongi, and A. Chieffi, Astrophys. J. **437**, 396 (1994).

[23] M. Hannam and W. Thompson, Nucl. Instrum. Methods Phys. Res. A **431**, 239 (1999).

[24] C. Angulo *et al.*, Nucl. Phys. **A656**, 3 (1999), also available online as NACRE compilation, http://pntpm.ulb.ac.be/nacre.htm

[25] Z. Mao and H. Fortune, Phys. Rev. C **50**, 2116 (1994).